Received: 28 June 2023 | Revised: 4 September 2023 | Accepted: 5 September 2023

DOI: 10.1111/ffe.14153

ORIGINAL ARTICLE

FFEMS Fatigue & Fracture of Engineering Materials & Structures WILEY

Closed-form solution for the *Fatemi-Socie* extended critical plane parameter in case of linear elasticity and proportional loading

Andrea Chiocca | **Michele Sgamma** | **Francesco Frendo**

Department of Civil and Industrial Engineering, University of Pisa, Pisa, Italy

Correspondence
Andrea Chiocca, Department of Civil and Industrial Engineering, University of Pisa, Pisa, Italy.
Email: andrea.chiocca@unipi.it

Funding information
Italian Ministry of University and Research, Grant/Award Number: CN00000023; European Union – NextGenerationEU

Abstract

Fatigue damage remains a significant issue for both metallic and non-metallic components, being the main cause of in-service failures. Among the different assessment methodologies, critical plane methods have gained significance as they enable identifying the critical location and the early crack propagation orientation. However, the standard plane scanning method used for calculating critical plane factors is computationally intensive, and as a result, it is usually applied only when the component's critical region is known in advance. In the presence of complex geometries, loads, or constraints, a more efficient method would be required. This work presents a closed-form solution to efficiently evaluate a critical plane factor based on the *Fatemi-Socie* criterion, in the case of isotropic linear-elastic material behavior and proportional loading conditions. The proposed algorithm, based on tensor invariants and coordinate transformation laws, was tested on different case studies under various loading conditions, showing a significant reduction in computation time compared to the standard plane scanning method.

KEYWORDS

closed-form solution, computational cost, critical plane, *Fatemi-Socie*, fatigue analysis, speed-up calculation

Highlights

- A closed-form solution for a critical plane factor based on *Fatemi-Socie* is presented.
- The method works in case of proportional loading and linear elasticity.
- The accuracy and efficiency of the method were proved against the usual procedure.
- A reduction greater than 99.8% in computation time was achieved.

1 | INTRODUCTION

The investigation of material's fatigue damage is a strategic subject of major relevance in several areas including academia and industry. Cumulative in-service fatigue loading is still one of the major causes of unexpected failures,[1] and it represents an important issue for designers. Although fatigue tests are often represented by simplified analyses, complexities such as stress/strain gradients, variable amplitude loading, randomness, and multiaxiality can easily be encountered in real cases.[2] Especially in such circumstances, finite element analysis (FEA) provides a valuable tool able to account for the complex features mentioned above.[3–8] The standard way to approach fatigue analysis consists of investigating the component's critical regions (i.e., considering stress/strain gradients and multiaxiality) and applying the correct loading history (i.e., accounting for variable amplitude or randomness). However, given the wide variety of geometries, loading conditions, and damage parameters to be considered, the solution of such models can be time-consuming during both the solution and post-processing phases.

While the complexity of geometry and boundary conditions is inherently related to the investigated problem and therefore unavoidable, the selection of the damage parameter, on the other hand, is a designer choice. Several methods exist to assess fatigue damage, among them two macro-categories can be identified: energy-based methods[9–12] and stress or strain-based methods.[13–20] Among the above mentioned categories, in the context of local damage methods, critical plane (CP) approaches gained a lot of popularity in recent years.[21–25] Methods based on critical plane require evaluating the plane orientation, which is subjected to the most severe damage. This orientation is defined as the critical plane and is representative of the orientation, at the material specific location, over which the crack should nucleate and initially propagate. Especially for the implementation of such damage parameters, large use of the FE method is made when dealing with complex geometry and loading histories. The standard way of evaluating the critical plane factor, however, requires the calculation of the damage factor over all possible plane orientations at each node of a FE model identifying the critical plane through a *blind-search-for* scanning process. Each plane orientation is identified by a set of two angles that are varied discretely by a fixed angular step to cover all the three-dimensional space. The processes is carried on for each node of the FE-model, usually throughout nested *for/end* loops, thus requiring significant computational power. Yet, the wide potential arising from such methodologies is currently limited due to their cumbersome implementation, and if compared to other widespread damage factors (e.g., nominal stress, hot spot stress, notch stress approach, etc.), critical plane methods are still confined to research and academia, being rarely used in the industry. The extensive computation time causes that only the critical zone of a component (e.g., notch) can be directly examined. However, this area may not always be identifiable a priori due to possible complex geometries, load histories, and constraints.

The main challenge during the computational process is to set the angular increment finding the right balance between accuracy and efficiency. Previous researches have focused on reducing the time needed for critical plane factor calculations. Some methods use analytical or semi-analytical techniques to determine the damage factor and the direction where it is maximized. A novel algorithm presented by Marques et al[26] utilizes analytical formulas to calculate only the spectral parameters related to the damage factor. Other approaches aim to increase computational speed by only calculating the critical plane factor in specific planes, rather than discretizing the entire space. Wentingmann et al[27] have developed an algorithm that increases the speed of critical plane detection by segmenting a coarse Weber half sphere with quad elements. Similarly, Sunde et al[28] developed an adaptive scheme that densifies a triangular mesh around the elements where the greatest damage has been observed. Sometimes instead, the loading condition of the specimen results in a reduced stress state that allows for a purely analytical formulation of the damage factor.[29–31]

This paper represents an extension of a previous paper published by the authors (Chiocca et al.[32]), where an analytical formulation to efficiently apply the critical plane method was developed for parameters that require the maximization of a single factor (e.g., the original formulation of *Fatemi-Socie*, which is based on the maximun shear strain range, *Smith-Watson-Topper*, *Kandil-Brown-Miller*, etc.). The analytical model presented in the following refers to the more general *Fatemi-Socie* formulation according to Jiang et al,[33] which is based on a combination of shear strain range and normal stress. Also in this case, indeed, under the assumption of proportional loading and linear-elastic material, a closed-form solution is possible. The model has been developed to be applied together with finite element analyses; for this reason, the constituent mathematics is based on a discrete formulation of the time history and the stress and strain tensors are defined for each generic loading condition. In the case of a complex load history, the method can be iteratively applied to each successive peak-to-valley, valley-to-peak pair derived from a specific cycle counting formulation. The first part of the paper explains the methodology in details, providing the necessary

theoretical background. In the second part of the paper, case studies are presented, including an hourglass specimen, a notched specimen and welded component under different loading conditions. A comparison is made between the standard method of calculating CP factors (i.e., plane scanning method) and the methodology presented in this work, in terms of solution accuracy and computational cost.

2 | GENERAL BACKGROUND ON CP FACTORS EVALUATION

Fatemi and Socie[34] as well as Fatemi and Kurath[35] introduced a multiaxial fatigue criterion based on the shear strain range. The parameter is mathematically defined in Equation (1):

$$\frac{\Delta\gamma}{2}\left(1+k\frac{\sigma_{n,max}}{S_y}\right) \tag{1}$$

where $\Delta\gamma$ represents the shear strain range acting over a given plane, $\sigma_{n,max}$ the maximum (i.e., over the load cycle/time interval) normal stress on the plane being evaluated, and S_y the material's yield strength. The material parameter k can be determined by comparing fatigue experimental data for uniaxial loading with data for pure torsion as described in Olausson.[36] Although certain authors suggest that the additional parameter k varies with the number of cycles to failure,[37–40] a constant value is considered for the present study. The fatigue parameter defined in Equation (1) is always positive, based on the fact that the shear strain range is considered as absolute value and considering that only positive normal stresses are taken into account (i.e., negative stresses are set equal to zero).

The original approach proposed by Fatemi and Socie[34] as well as Fatemi and Kurath[35] identified the critical plane as the one experiencing the maximum shear strain range $\Delta\gamma_{max}$, disregarding the terms in parantheses. Following this approach, the fatigue parameter to be used is given by

$$FS' = \frac{\Delta\gamma_{max}}{2}\left(1+k\frac{\sigma_{n,max}}{S_y}\right) \tag{2}$$

An analytical solution for such criterion has been the subject of previous articles published by the authors.[32,41] In the current investigation, instead, as made by some other authors (e.g., Jiang et al.[33]), the critical plane is defined as the plane where the entire fatigue parameter (FS) expressed in Equation (3) reaches its maximum value, that is:

$$FS = \max\left[\frac{\Delta\gamma}{2}\left(1+k\frac{\sigma_{n,max}}{S_y}\right)\right] \tag{3}$$

The critical plane defined in this way generally has a different orientation, if compared to the critical plane defined considering only the maximum of the shear strain range, as it also depends on the normal stress. This is a different case, where a closed-form solution is still possible, under more restrictive hypothesis, as it will be discussed in Section 4.

3 | EVALUATING THE CP FACTOR USING THE STANDARD PLANE SCANNING TECHNIQUE

In this section, the standard procedure for determining the CP factor through the plane scanning technique is briefly recalled, as presented in Figure 1. The time-varying stress $\boldsymbol{\sigma}(t)$ and strain $\boldsymbol{\varepsilon}(t)$ tensors can be obtained at each node in a FE-model in a general reference frame $Oxyz$:

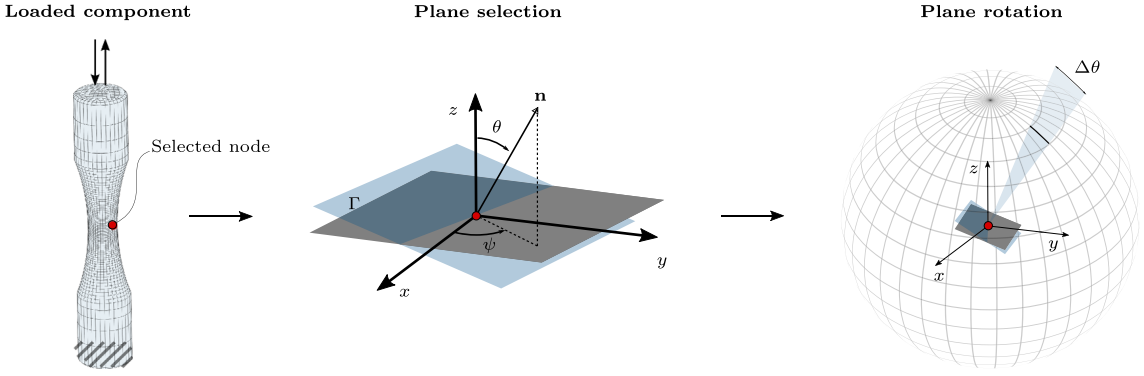

FIGURE 1 Standard procedure sequence to assess a critical plane factor by plane scanning method. [Colour figure can be viewed at wileyonlinelibrary.com]

$$\boldsymbol{\sigma}(t)=\begin{bmatrix}\sigma_{xx}(t) & \tau_{xy}(t) & \tau_{xz}(t)\\ \tau_{yx}(t) & \sigma_{yy}(t) & \tau_{yz}(t)\\ \tau_{zx}(t) & \tau_{zy}(t) & \sigma_{zz}(t)\end{bmatrix},$$
$$\boldsymbol{\varepsilon}(t)=\begin{bmatrix}\varepsilon_{xx}(t) & \frac{\gamma_{xy}}{2}(t) & \frac{\gamma_{xz}}{2}(t)\\ \frac{\gamma_{yx}}{2}(t) & \varepsilon_{yy}(t) & \frac{\gamma_{yz}}{2}(t)\\ \frac{\gamma_{zx}}{2}(t) & \frac{\gamma_{zy}}{2}(t) & \varepsilon_{zz}(t)\end{bmatrix} \quad (4)$$

Stress and strain tensors can be utilized to describe various types of loading conditions, such as uniaxial, biaxial, or multiaxial; in addition, the load time history can exhibit proportional or non proportional stress and strain components. It is possible to calculate stress and strain values acting on different plane orientations, that is, by considering different reference coordinate systems, using simple matrix operation $R^T\boldsymbol{\sigma}R$, where R represents the rotation matrix. Actually, two angular coordinates, say θ and ψ, are strictly necessary to identify a plane orientation. In this sense there are ∞^2 possible orientation at each location to be checked. By incrementally rotating the plane (or its unit vector) through fixed angular increments (i.e., $\Delta\theta$ and $\Delta\psi$), stress and strain values in all directions can be approximately obtained. Once this process has been carried out, the plane that maximizes the reference CP parameter can be identified as the critical plane. The above mentioned procedure requires to implement nested *for/end* loops and this results highly inefficient from a computational point of view, depending on the selected angular resolution. This becomes even more critical when trying to perform this analysis for many points in the component (i.e., nodes in the FE model).

For the present study, a rotation sequence in a moving reference frame was considered, the first rotation ψ about the z-axis and the second rotation θ about the y-axis, as shown in Equation (5), and the plane scanning method was applied through angular steps $\Delta\theta$ and $\Delta\psi$ of 1°.

$$R=R_z(\psi)R_y(\theta)=\begin{bmatrix}\cos(\theta)\cos(\psi) & -\sin(\psi) & \cos(\psi)\sin(\theta)\\ \sin(\psi)\cos(\theta) & \cos(\psi) & \sin(\theta)\sin(\psi)\\ -\sin(\theta) & 0 & \cos(\theta)\end{bmatrix} \quad (5)$$

Through the rotation matrix R, it is possible to retrieve the stress and strain tensors in the rotated reference frame as presented in Equation (6).

$$\boldsymbol{\sigma}'=R^T\boldsymbol{\sigma}R,\ \boldsymbol{\varepsilon}'=R^T\boldsymbol{\varepsilon}R \quad (6)$$

4 | CLOSED-FORM SOLUTION

In this section, the mathematical framework of the method is outlined. As the method was developed for a finite element modeling-related application, the load history is described by a discrete formulation of the time sequence, via load steps in a FE-analysis. To this regard, the relationships of Equation (7) give the stress and strain tensors at the generic i-th loading step.

$$\boldsymbol{\sigma}^{(i)}=\begin{bmatrix}\sigma_{xx} & \tau_{xy} & \tau_{xz}\\ \tau_{yx} & \sigma_{yy} & \tau_{yz}\\ \tau_{zx} & \tau_{zy} & \sigma_{zz}\end{bmatrix}^{(i)},\ \boldsymbol{\varepsilon}^{(i)}=\begin{bmatrix}\varepsilon_{xx} & \frac{\gamma_{xy}}{2} & \frac{\gamma_{xz}}{2}\\ \frac{\gamma_{yx}}{2} & \varepsilon_{yy} & \frac{\gamma_{yz}}{2}\\ \frac{\gamma_{zx}}{2} & \frac{\gamma_{zy}}{2} & \varepsilon_{zz}\end{bmatrix}^{(i)} \quad (7)$$

Starting from the above tensors, the strain range tensor between the i-th and $i+1$-th loading conditions can be easily determined, as shown in Equation (8); in order to compute the strain range tensor, the starting tensors have to be defined with respect to the same reference frame, but this is fairly common within the post-processing phase of FE-analyses.

$$\Delta\varepsilon^{(i,i+1)}=\boldsymbol{\varepsilon}^{(i)}-\boldsymbol{\varepsilon}^{(i+1)}=\begin{bmatrix}\Delta\varepsilon_{xx} & \frac{\Delta\gamma_{xy}}{2} & \frac{\Delta\gamma_{xz}}{2}\\ \frac{\Delta\gamma_{yx}}{2} & \Delta\varepsilon_{yy} & \frac{\Delta\gamma_{yz}}{2}\\ \frac{\Delta\gamma_{zx}}{2} & \frac{\Delta\gamma_{zy}}{2} & \Delta\varepsilon_{zz}\end{bmatrix}^{(i,i+1)} \quad (8)$$

Under the hypotheses of linear isotropic elasticity and proportional loading, the following deductions hold:

- the stress and strain tensors have the same principal directions, that is, the same eigenvectors;
- the strain tensors (as well as the stress tensor), evaluated at different time steps, (i) and $(i+1)$ have the same principal directions, that is, the same eigenvectors.

From the above considerations, it follows that also the strain range tensor $\Delta\varepsilon^{(i,i+1)}$ (as well as, for example the stress range tensor in case of the *Findley* criterium) has the same principal directions of the strain or the stress tensors, evaluated at the i-th and $i+1$-th time steps.

On the basis of the coincidence between the principal directions of the tensors $\boldsymbol{\sigma}^{(i)}$, $\boldsymbol{\sigma}^{(i+1)}$, $\boldsymbol{\varepsilon}^{(i)}$, $\boldsymbol{\varepsilon}^{(i+1)}$ and $\Delta\varepsilon^{(i,i+1)}$, it is now useful to refer to the Mohr's circular representation to further illustrate the method.

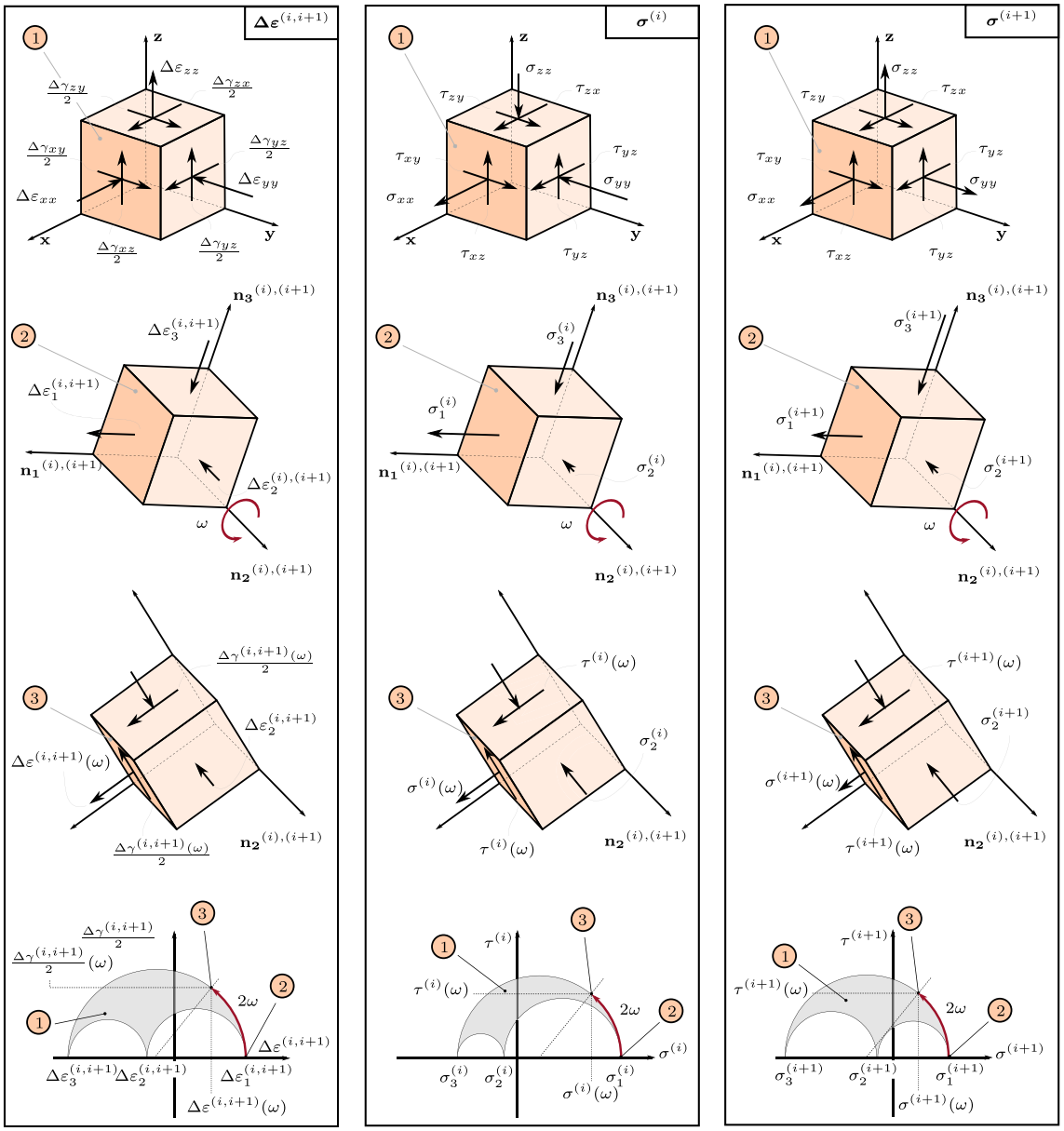

FIGURE 2 Graphical representation of the analytical method by Cauchy elementary cube and Mohr's circle by means of the tensors $\Delta\boldsymbol{\varepsilon}^{(i,i+1)}$, $\boldsymbol{\sigma}^{(i)}$, and $\boldsymbol{\sigma}^{(i+1)}$ [Colour figure can be viewed at wileyonlinelibrary.com]

Figure 2 represents the tensor quantities, which are present in the *Fatemi-Socie* critical plane method (see Equation 1), namely, $\Delta\boldsymbol{\varepsilon}^{(i,i+1)}$, $\boldsymbol{\sigma}^{(i)}$, and $\boldsymbol{\sigma}^{(i+1)}$. As a first step, all the stress and strain components have to be obtained (at a given node in the FE model) in a given, typically the global, reference frame *Oxyz*. Then, an *eigenvalue–eigenvector* analysis is required for the strain range tensor $\Delta\boldsymbol{\varepsilon}^{(i,i+1)}$; the so obtained *eigenvalues* (i.e., $\Delta\varepsilon_1^{(i,i+1)}$, $\Delta\varepsilon_2^{(i,i+1)}$, and $\Delta\varepsilon_3^{(i,i+1)}$) represent the principal parameters of the strain range, while the *eigenvectors* define the principal directions $\boldsymbol{n_1}^{(i),(i+1)}$, $\boldsymbol{n_2}^{(i),(i+1)}$, and $\boldsymbol{n_3}^{(i),(i+1)}$ of the $\Delta\boldsymbol{\varepsilon}^{(i,i+1)}$ tensor.

As previously stated, these unit vectors also represent the principal directions (i.e., *eigenvectors*) of the tensors $\boldsymbol{\sigma}^{(i)}$ and $\boldsymbol{\sigma}^{(i+1)}$. Therefore, the three tensors $\Delta\boldsymbol{\varepsilon}^{(i,i+1)}$, $\boldsymbol{\sigma}^{(i)}$, and $\boldsymbol{\sigma}^{(i+1)}$ expressed in the principal reference frame $On_1n_2n_3$ are represented by their principal components:

- $\Delta\varepsilon_1^{(i,i+1)}$, $\Delta\varepsilon_2^{(i,i+1)}$, $\Delta\varepsilon_3^{(i,i+1)}$ for $\Delta\boldsymbol{\varepsilon}^{(i,i+1)}$ tensor;
- $\sigma_1^{(i)}$, $\sigma_2^{(i)}$, $\sigma_3^{(i)}$ for $\boldsymbol{\sigma}^{(i)}$ tensor;
- $\sigma_1^{(i+1)}$, $\sigma_2^{(i+1)}$, $\sigma_3^{(i+1)}$ for $\boldsymbol{\sigma}^{(i+1)}$ tensor;

with the usual convention $\alpha_1 > \alpha_2 > \alpha_3$, α representing the generic *eigenvalue*.

Finally, on the basis of the Mohr's circular representation, the FS parameter can be obtained as follows. The analytical expression of $\frac{\Delta\gamma}{2}^{(i,i+1)}$, as a function of the ω angle, which represents a rotation about the n_2 principal direction (see Figure 2), is given by the following relationship 9.

$$\frac{\Delta\gamma^{(i,i+1)}(\omega)}{2} = \left(\frac{\Delta\varepsilon_1^{(i,i+1)} - \Delta\varepsilon_3^{(i,i+1)}}{2}\right)\sin(2\omega) \tag{9}$$

Considering the normal stress acting on the plane identified by the ω angle, the maximum value among the two conditions (i) and $(i+1)$ of the load cycle have to be considered:

$$\sigma_{n,max}^{(i),(i+1)}(\omega) = \max_{\{(i),(i+1)\}}\left[\left(\frac{\sigma_1+\sigma_3}{2}\right) + \left(\frac{\sigma_1-\sigma_3}{2}\right)\cos(2\omega)\right]^{(i),(i+1)} \tag{10}$$

From Figure 2, it can be observed that the maximum normal stress can belong either to the (i)-th time step, or the $(i+1)$-th time step, depending on the plane orientation ω. In order to solve the following maximization problem, represented by Equation (11),

$$FS(\omega) = \max_{\{\omega\}}\left[\frac{\Delta\gamma^{(i,i+1)}(\omega)}{2}\left(1 + k\frac{\sigma_{n,max}^{(i),(i+1)}(\omega)}{S_y}\right)\right] \tag{11}$$

the following parameters are introduced:

$$\begin{cases} a = \left(\dfrac{\Delta\varepsilon_1^{(i,i+1)} - \Delta\varepsilon_3^{(i,i+1)}}{2}\right) \\ b = \left(\dfrac{\sigma_1+\sigma_3}{2S_y}\right)^{(i),(i+1)} \\ c = \left(\dfrac{\sigma_1-\sigma_3}{2S_y}\right)^{(i),(i+1)} \end{cases} \tag{12}$$

Parameter a represents the diameter of the largest strain range circle in Figure 2; parameter b represents the center of the largest stress circle, normalized with respect to the yield stress; parameter c represents the diameter of the largest stress circle, normalized with respect to the yield stress. It should be noted that a is referenced to the load cycle, while b and c has to be evaluated for (i)-th and $(i+1)$-th time step. Parameters a and c are always positive according to the standard convention on the *eigenvalues* ($\Delta\varepsilon_1 \geq \Delta\varepsilon_2 \geq \Delta\varepsilon_3$ and $\sigma_1 \geq \sigma_2 \geq \sigma_3$), while b can be either positive or negative.

After substituting the parameters of Equation (12) into Equation (11), the maximum value of FS parameter can be determined by carrying out an analytical derivative of the $FS(\omega)$ function, as presented in Equation (13), with respect to ω.

$$FS = \max_{\{\omega\}}\left[a\sin(2\omega)(1 + k(b + c\cos(2\omega)))\right] \tag{13}$$

It is worth noting that, generally, two critical plane orientations can always be obtained. Indeed, in case the eigenvalues $\Delta\varepsilon_1^{(i,i+1)}$, $\Delta\varepsilon_2^{(i,i+1)}$, and $\Delta\varepsilon_3^{(i,i+1)}$ are all different from each other, the algorithm identifies two critical planes associated with the same maximum value FS, as

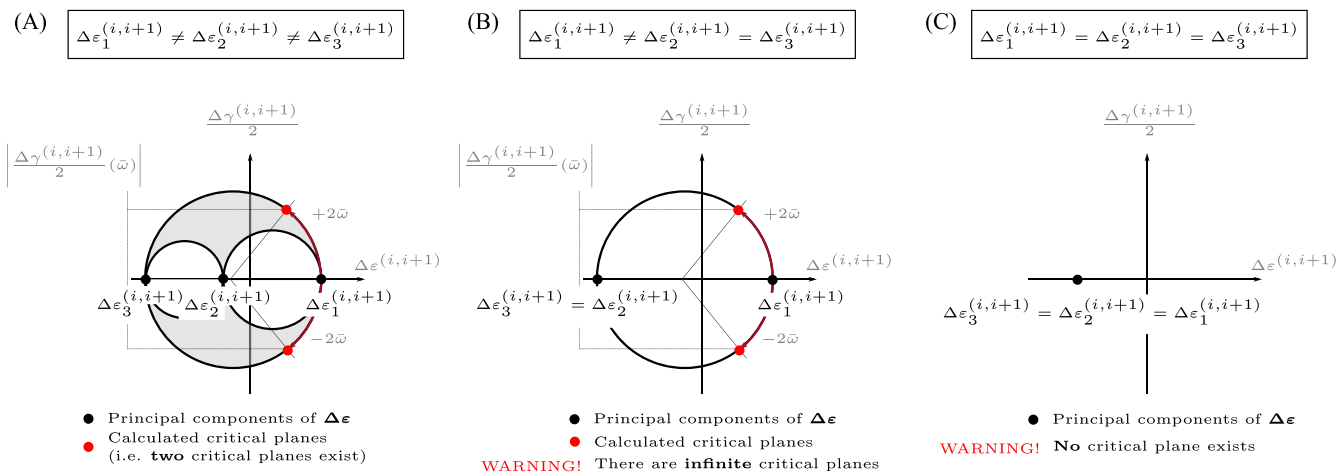

FIGURE 3 Representation, by means of the Mohr circles, of the different number of existing critical planes for proportional loading scenarios. [Colour figure can be viewed at wileyonlinelibrary.com]

presented in Figure 3A. With reference to the circular representation, this occurs for two points located on the largest circle related to the strain ranges, having the same normal strain range (and also the same normal stress $\sigma_{n,max}$), since the absolute value of $\Delta\gamma^{(i,i+1)}$ is accounted for in the fatigue parameter FS. These planes are identified by rotating by the angles $+2\overline{\omega}$ and $-2\overline{\omega}$ on the maximum Mohr's circle, with respect to the plane having the maximum principal strain range. As $\pm2\overline{\omega}$ angles are associated with the same maximum normal stress, the same FS is obtained.

There are some special cases with more than two critical planes. For example, when there are two identical eigenvalues of the stress tensors at load step i and load step $i+1$ (i.e., uniaxial or equibiaxial state of stress). In this case also, the strain range tensor $\Delta\varepsilon^{(i,i+1)}$ has two identical eigenvalues, and there exist infinite critical plane orientations associated with the same FS value. In fact, the points identified in Figure 3B by the angles $\pm2\overline{\omega}$ can be considered to be obtained by a rotation about either the direction identified by the eigenvector $\boldsymbol{n_2}$ or the direction identified by the eigenvector $\boldsymbol{n_3}$ in case of uniaxial state of stress, or by a rotation about either the direction identified by the eigenvector $\boldsymbol{n_1}$ or the direction identified by the eigenvector $\boldsymbol{n_2}$ in case of equibiaxial state of stress. In both cases, any direction that can obtained by a linear combination of $\boldsymbol{n_2}$ or $\boldsymbol{n_3}$ (uniaxial) and $\boldsymbol{n_1}$ or $\boldsymbol{n_2}$ (equibiaxial) identifies a critical plane as well. This is, for example, the case of an axisymmetric specimen under axisymmetric load condition. Another special case is that of an alternate shear load condition, such as a round specimen under alternate torsion. In this case, there are two opposite eigenvalues of the strain range tensor $\Delta\varepsilon_1^{(i,i+1)} = -\Delta\varepsilon_3^{(i,i+1)}$ and two opposite eigenvalues of the stress tensor at load step i (i.e., $\sigma_1^{(i)} = -\sigma_3^{(i)}$) and at load step $i+1$ (i.e., $\sigma_1^{(i+1)} = -\sigma_3^{(i+1)}$). Under these conditions, for each point determined by $\pm2\overline{\omega}$ in the circular representation, there are two critical planes since the maximum (positive) normal stress acts on a given plane at i load-step and on the conjugate plane (orthogonal to the previous one) at $i+1$ load step. Furthermore, as presented in Figure 3C, if an hydrostatic state of stress occurs, there are three identical eigenvalues, and no critical plane exists since there is no shear strain and being $FS = 0$.

The rotation matrices to be considered for identifying the critical plane orientation are given in Equation (14), and they are obtained considering the product of the rotation matrix R_p, representing the matrix containing the direction cosines related to the principal directions, with the rotation matrix R_y, representing the rotation about the local y-axis of an angle $\pm\overline{\omega}$.

$$R = R_p R_y(\pm\overline{\omega}) = \begin{bmatrix} | & | & | \\ \boldsymbol{n_1}^{(i),(i+1)} & \boldsymbol{n_2}^{(i),(i+1)} & \boldsymbol{n_3}^{(i),(i+1)} \\ | & | & | \end{bmatrix} \begin{bmatrix} \cos(\pm\overline{\omega}) & 0 & \sin(\pm\overline{\omega}) \\ 0 & 1 & 0 \\ -\sin(\pm\overline{\omega}) & 0 & \cos(\pm\overline{\omega}) \end{bmatrix} \tag{14}$$

In the following, for the sake of simplicity, the treatise will refer to the solution obtained for the plane identified by $+\overline{\omega}$. Similar relationships hold for the plane identified by $-\overline{\omega}$.

The result of the maximization problem defined in previous Equation (13) in terms of $\overline{\omega}$ and FS are given in the following Equations (15)–(16):

$$\overline{\omega} = \begin{cases} \frac{1}{2}\arctan\left(\dfrac{\dfrac{\sqrt{2}\sqrt{\dfrac{k\left(b(d-2)+b^2(-k)+4c^2k\right)+d-1}{ck}}}{\sqrt{c}\sqrt{k}}}{\dfrac{d-bk-1}{ck}}\right) & b \geq -\dfrac{1}{k} \\ \frac{1}{2}\arctan\left(\dfrac{-\dfrac{\sqrt{2}\sqrt{-\dfrac{k\left(b(d+2)+b^2k-4c^2k\right)+d+1}{ck}}}{\sqrt{c}\sqrt{k}}}{-\dfrac{d+bk+1}{ck}}\right) & b \leq -\dfrac{1}{k} \end{cases} \tag{15}$$

$$FS = \begin{cases} \dfrac{a(d+3bk+3)\sqrt{\dfrac{k\left(b(d-2)+b^2(-k)+4c^2k\right)+d-1}{ck}}}{8\sqrt{2}\sqrt{c}\sqrt{k}} & b \geq -\dfrac{1}{k} \\ \dfrac{a(d-3bk-3)\sqrt{-\dfrac{k\left(b(d+2)+b^2k-4c^2k\right)+d+1}{ck}}}{8\sqrt{2}\sqrt{c}\sqrt{k}} & b \leq -\dfrac{1}{k} \end{cases} \tag{16}$$

where $d = \left(\sqrt{k^2\left(b^2+8c^2\right)+2bk+1}\right)^{(i),(i+1)}$ represents an aggregative parameter to simplify the formula structure. It has to be noted that the analytical expression of Equations (15)–(16) have to be evaluated for both (i) and $(i+1)$ load cycles, and then, the FS CP factor is selected as the solution having the maximum (always positive) value.

As it can be observed, both $\overline{\omega}$ and FS are characterized by a C^0-type continuity condition at $b = -\frac{1}{k}$.

An example of the solution for a structural steel having $S_y = 355$ MPa is given in Figure 4. The solution is given for two fixed values of the material constant $k = 0.1$ and $k = 1$, which represent typical extreme values for that parameter. The stress-strain state involved in the loading cycle is described by parameters a, b, c given in previous

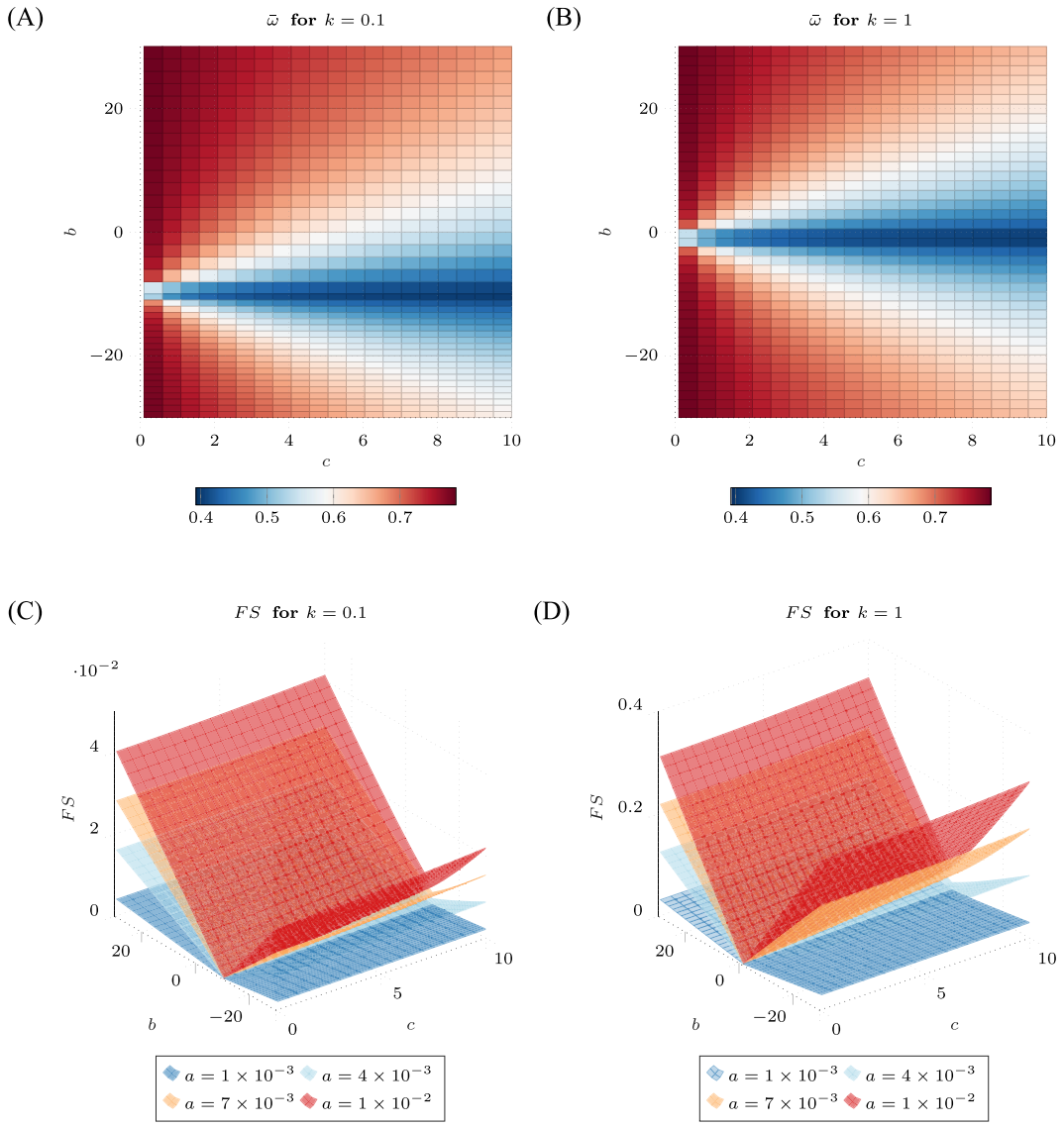

FIGURE 4 Surface plots of $\overline{\omega}$ and FS functions (A) $\overline{\omega}$ for $k = 0.1$, (B) $\overline{\omega}$ for $k = 1$, (C) FS for $k = 0.1$ and $a = [0.001, 0.004, 0.007, 0.01]$, and (D) FS for $k = 1$ and $a = [0.001, 0.004, 0.007, 0.01]$ [Colour figure can be viewed at wileyonlinelibrary.com]

Equation (12); in other words, each point on the surface represent a different fatigue loading scenario. Figure 4A, B reports the $\overline{\omega}$ function, while the FS function is shown in Figure 4C,D for $k = 0.1$ and $k = 1$, respectively. It can be observed how the $\overline{\omega}$ solution can be represented through an individual surface, being independent of the value of a, that is, on the shear strain range.

On the other hand, the FS parameter is strongly influenced by the shear strain range, represented by parameter a and moderately influenced by parameter b representing the normalized radius of the largest stress circle. The influence of parameter c on the FS parameter is much lower in all the domain. The effect of k can be clearly noticed, for $b = -\frac{1}{k}$, in all the plots.

In order to enable a direct graphical comparison between the analytical formulation and the plane scanning method, the same rotation sequence of Equation (5) can be employed, as presented in the following:

$$R = R_z(\psi)R_y(\theta) = \begin{bmatrix} r_{11} & r_{12} & r_{13} \\ r_{21} & r_{22} & r_{23} \\ r_{31} & r_{32} & r_{33} \end{bmatrix} \tag{17}$$

On the basis of Equations (5), (14), and (17), a possible way to obtain the two angles (θ and ψ) in analytical form is shown in Equation (18).

$$\begin{aligned} \theta &= \arctan2\left(\sqrt{r_{13}^2 + r_{23}^2}, r_{33}\right) \\ \psi &= \arctan2(r_{23}, r_{13}) \end{aligned} \tag{18}$$

5 | MATERIAL AND METHOD

In order to validate the analytical solution presented in the previous section, three different case studies were selected, to represent a wide range of structural problems that may be found in practical applications. The case studies include an hourglass specimen, a notched specimen, and a welded joint between a pipe and a plate. The hourglass and notched specimens were subjected to tensile-compressive and torsional loading, while the welded joint was subjected to pure bending and pure torsional loading. The technical drawing of the hourglass specimen, based on ASTM E466 with a minimum diameter of 12 mm, is shown in Figure 5A. The notched specimen geometry, described by a notch radius of 0.2 mm and a minimum diameter of 16 mm, is shown in Figure 5B. Figure 5C shows the welded joint geometry, which consists of a tube, a reinforcement circular plate, and a quadrangular base plate. The seam weld of interest for this work was the one between the tube and the base plate. The welded joint was previously studied by the same authors examining its fatigue endurance under different loading conditions and in the presence of residual stresses.[4-6,42-45] For all the cases, FE-analyses were conducted using the second release of Ansys© 2021 software. Static structural analyses were performed assuming small displacements; structural steel S355 was considered as the material for all three case studies with linear elastic

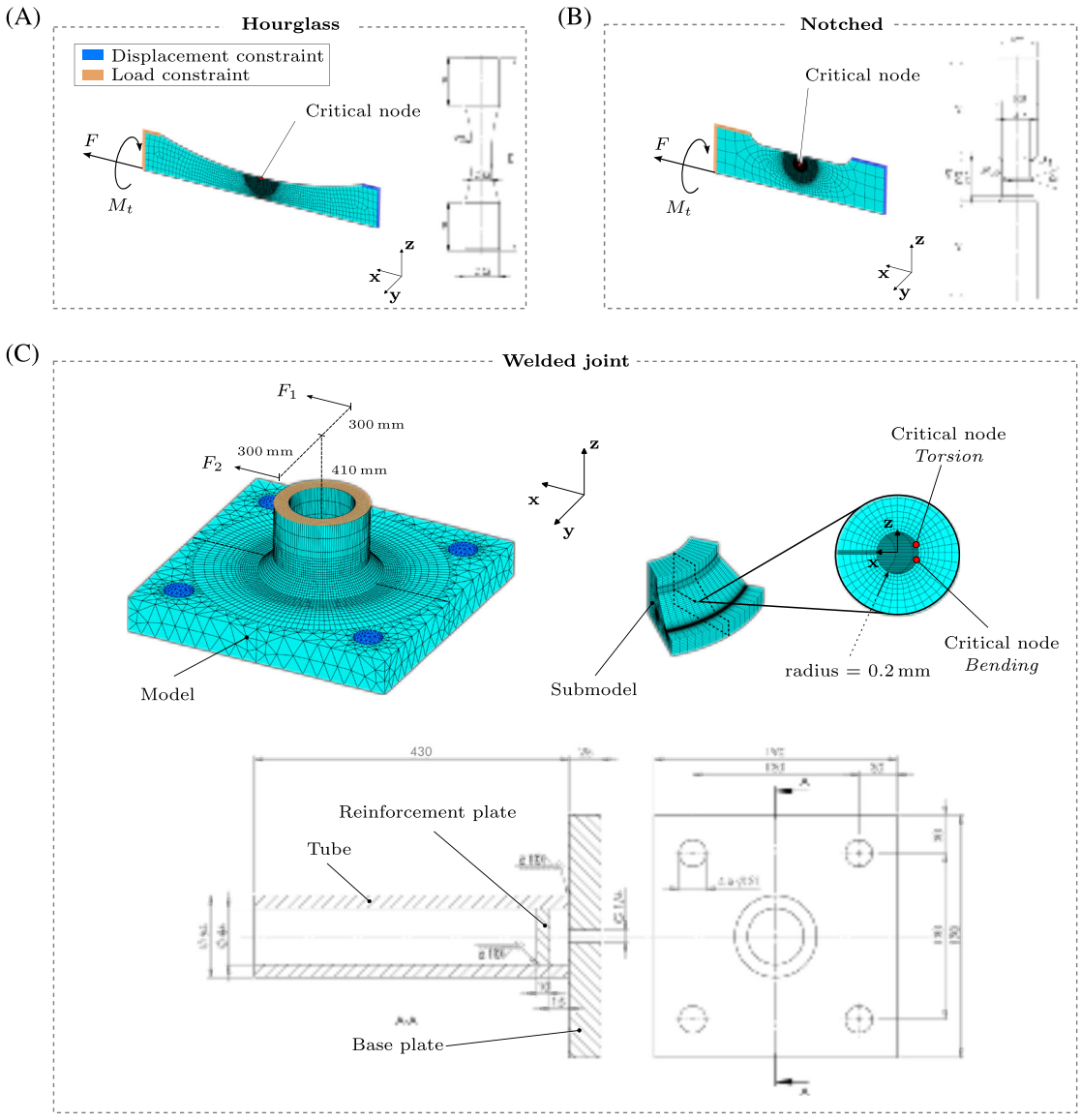

FIGURE 5 Finite element models and technical drawings of the investigated case studies: (A) two-dimensional model of the hourglass specimen, (B) two-dimensional model of the notched specimen, and (C) welded joint with model and submodel. [Colour figure can be viewed at wileyonlinelibrary.com]

TABLE 1 Load steps combination used during simulations to apply proportional loading conditions with F, F_1, and F_2 referring to the applied forces and M_t referring to the torque shown in Figure 5.

	Hourglass specimen		Notched specimen		Welded joint	
Load type	**Load step n.1**	**Load step n.2**	**Load step n.1**	**Load step n.2**	**Load step n.1**	**Load step n.2**
Case 1	$F = 19\,\text{kN}$	$F = 76\,\text{kN}$	$F = 5.3\,\text{kN}$	$F = 53\,\text{kN}$	$F_1 = 5.7\,\text{kN}$	$F_1 = 5.7\,\text{kN}$
	$M_t = 0\,\text{N m}$	$M_t = 0\,\text{N m}$	$M_t = 0\,\text{N m}$	$M_t = 0\,\text{N m}$	$F_2 = 5.7\,\text{kN}$	$F_2 = 5.7\,\text{kN}$
Case 2	$F = 0\,\text{kN}$	$F = 0\,\text{kN}$	$F = 0\,\text{kN}$	$F = 0\,\text{kN}$	$F_1 = -14.9\,\text{kN}$	$F_1 = 14.9\,\text{kN}$
	$M_t = 10\,\text{N m}$	$M_t = 100\,\text{N m}$	$M_t = 10\,\text{N m}$	$M_t = 80\,\text{N m}$	$F_2 = 14.9\,\text{kN}$	$F_2 = -14.9\,\text{kN}$

TABLE 2 Overview of the main normal and shear stress components pattern over load steps; stress components are based on the reference frames reported in Figure 5.

Load type	Hourglass specimen	Notched specimen	Welded joint
Case 1	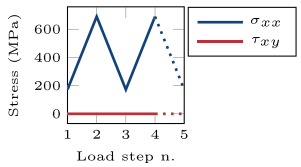	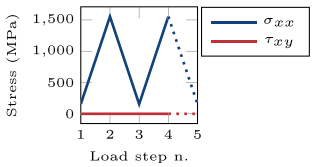	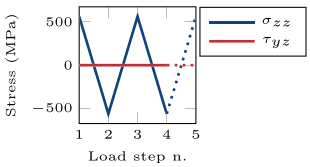
Case 2	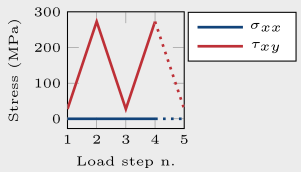	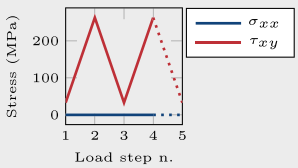	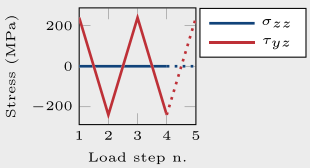

behavior, $E = 210\text{GPa}$ and $\nu = 0.3$. In order to determine the FS critical plane factor, a yield strength $S_y = 355\text{MPa}$ and a material constant $k = 0.4$ were considered.

A three-dimensional FE model was used for the welded joint with 3D structural brick elements (i.e., SOLID185) with 20 nodes and a quadratic shape function. Whereas, in the case of hourglass and notched specimens, an axisymmetric model was employed together with 2D structural plane elements (i.e., PLANE183)* with eight nodes and a quadratic shape function. The mesh size for all FE models was achieved after a convergence analysis by attaining a difference lower than 5% on the maximum von Mises stress.

The loading conditions were obtained by applying forces or moments together with fixed supports on the appropriate model surfaces. In the case of hourglass and notched specimens, the outer regions of the models were used for applying the boundary conditions, while the top tube surface and the plate holes were used in the case of the welded joint.

The load sequences reported in Tables 1 and 2 were applied, consisting of two proportional loading conditions. Each column of Table 1 reports the combination of forces/moment applied to a specific specimen geometry in a particular load step of the FE-simulation.

*Element keyoption(3) = 1 for tension-compression loading and element keyoption(3) = 6 for torsion loading.

6 | RESULTS

In this section, the FS closed-form solution results are discussed in comparison with those obtained by using the standard plane scanning method. The functions presented in Section 4 provide the essential mathematical background to apply the analytical method; the CP factor solutions resulting from the above functions furnish the results explicitly, yielding a precise solution rather than a numerical approximation.

Figure 6 provides a graphical comparison of CP orientation and CP values between the two methods for the three different loading cases presented in the previous section, including the hourglass specimen, notched specimen, and welded joint. To provide a complete overview of the results, the FS values are reported in Table 3 to allow a direct comparison between the employed methods. The tensile loading case for the hourglass and notched specimens, as well as the bending loading case for the welded joint, are shown in Figure 6A–C, while the torsional loading cases are presented in Figure 6D–F, respectively. The CP orientations identified by the

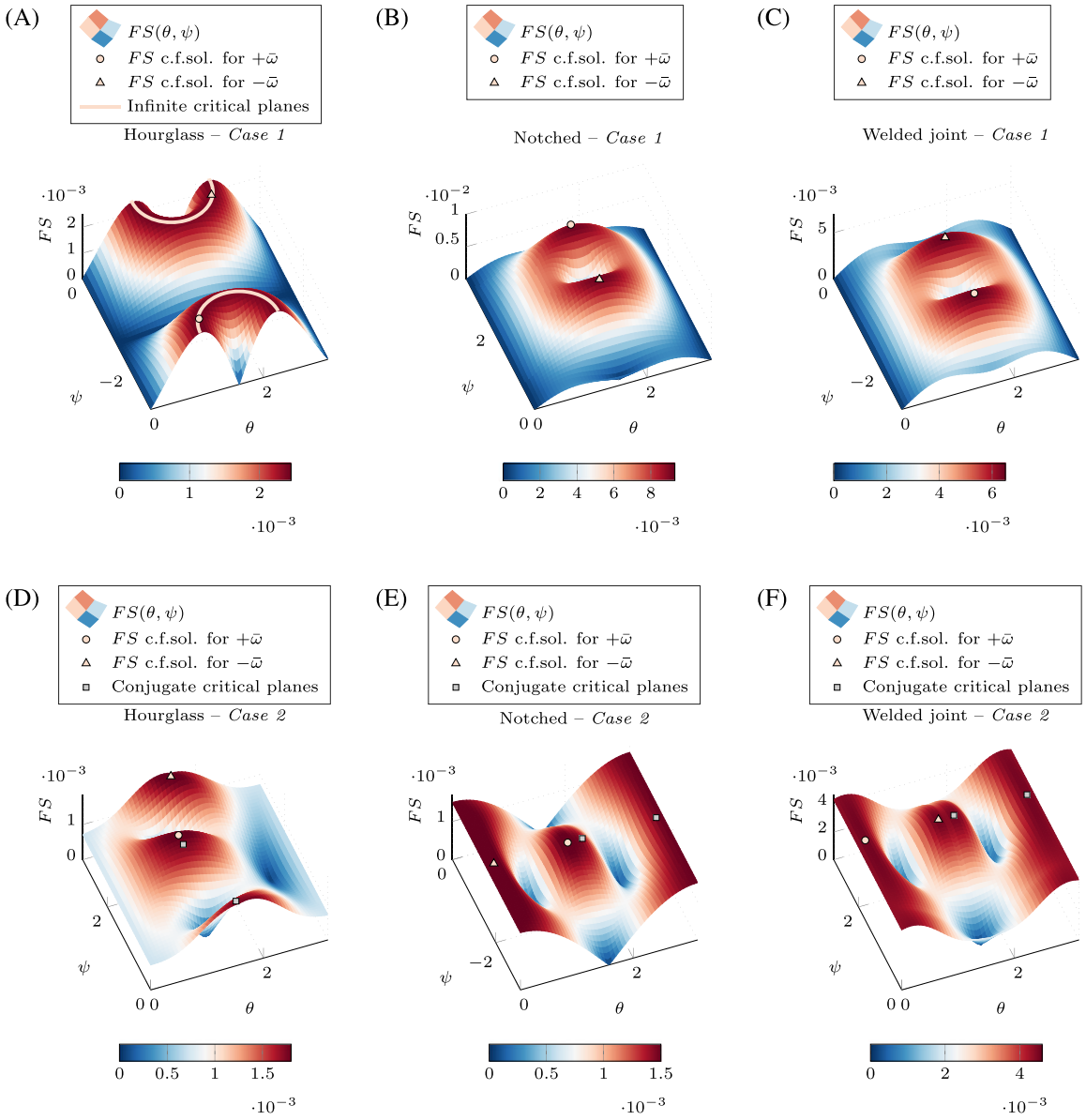

FIGURE 6 Comparison of FS solutions between the standard plane scanning method $FS(\theta,\psi)$ and that derived from the closed-form solution (i.e., c.f.sol.) FS for (A) the hourglass specimen subjected to tensile loading, (B) the notched specimen subjected to tensile loading, (C) the welded joint subjected to bending loading, (D) the hourglass specimen subjected to torsion loading, (E) the notched specimen subjected to torsion loading, and (F) the welded joint subjected to torsion loading. [Colour figure can be viewed at wileyonlinelibrary.com]

closed-form solution are represented though circular and triangular marks in all the figures. As it can be observed, the closed-form solution perfectly fits with the maximum shown in Table 3 and in Figure 6 as colored surfaces, which represent the $FS(\theta,\psi)$ values derived from the spatial plane scanning method. The surfaces exhibit periodicity by repeating the same pattern every π radiant over both θ and ψ angular directions. Nevertheless, the solution found by the proposed closed-form solution can identify all the maximum by considering the function periodicity. In fact, in the case of opposite eigenvalues of $\Delta\varepsilon^{(i,i+1)}$ (i.e., alternate torsion), the additional critical planes are represented by the squares in Figure 6D–F, found by imposing a periodicity of $\frac{\pi}{2}$ on $\pm\overline{\omega}$. The values of parameters a, b, and c are reported in Table 4 for the case-studies presented in Figure 6A–F.

The improvement in computing time is illustrated in Table 5. All codes were executed in the Matlab® environment on an 11th Gen. Intel(R) Core(TM) i7 with 16GB of available RAM and 4 cores. The performance index PI defined in Equation (19) was used to compare the computational efficiency of the closed-form solution, to the standard plane scanning method. In Equation (19), t_{cs} represents the computation time

TABLE 3 Comparison of *FS* values and critical plane orientations between the closed-form solution and the standard plane scanning method for proportional loading conditions.

***FS* comparison ($\pm\bar{\omega}$)**						
	Hourglass specimen		**Notched specimen**		**Welded joint**	
Load type	**Closed-form**	**Standard**	**Closed-form**	**Standard**	**Closed-form**	**Standard**
Case 1	2.42×10^{-3}	2.42×10^{-3}	9.20×10^{-3}	9.20×10^{-3}	6.45×10^{-3}	6.45×10^{-3}
Case 2	1.83×10^{-3}	1.83×10^{-3}	1.55×10^{-3}	1.55×10^{-3}	4.53×10^{-3}	4.53×10^{-3}

***θ* and *ψ* comparison ($+\bar{\omega}$)**												
	Hourglass specimen				**Notched specimen**				**Welded joint**			
	Closed-form		**Standard**		**Closed-form**		**Standard**		**Closed-form**		**Standard**	
Load type	θ	ψ	θ	ψ	θ	ψ	θ	ψ	θ	ψ	θ	ψ
Case 1	0.975	−2.83	-[a]	-[a]	1.570	2.41	1.571	2.42	1.570	−2.40	1.570	−2.39
Case 2	1.156	1.727	1.155	1.727	1.440	−1.570	1.442	−1.571	0.1367	2.04	0.1363	2.05

***θ* and *ψ* comparison ($-\bar{\omega}$)**												
	Hourglass specimen				**Notched specimen**				**Welded joint**			
	Closed-form		**Standard**		**Closed-form**		**Standard**		**Closed-form**		**Standard**	
Load type	θ	ψ	θ	ψ	θ	ψ	θ	ψ	θ	ψ	θ	ψ
Case 1	2.16	−0.304	-[a]	-[a]	1.570	1.090	1.571	1.091	1.57	−1.053	1.56	−1.054
Case 2	1.512	3.01	1.516	3.02	0.1301	−1.572	0.1303	−1.571	1.434	2.04	1.427	2.05

[a]Infinite solutions exist.

TABLE 4 Parameter values required to calculate the *FS* closed-form solution for all case studies described in Figure 6.

Case study	***a***	***b***	***c***
Hourglass – Tensile	0.0017	0.9729	0.9731
Notched – Tensile	0.0121	0.7041	0.6218
Welded joint – Bending	0.0046	0.8835	0.8296
Hourglass – Torsion	0.0018	0	0.0843
Notched – Torsion	0.0015	0	0.7415
Welded joint – Torsion	0.0043	0	0.7903

required by the closed-form solution, while t_{ps} represents the computation time required by the plane scanning procedure. *PI* is 100% when the computation time of the closed-form solution is zero, or when the computation time required by the plane scanning method is infinite, and 0% when there is no reduction in computing time, that is, $t_{cs} = t_{ps}$. The significant time reduction is caused by avoiding multiple plane scanning in space while providing the exact solution. As it can be observed, significant time reduction was achieved, with the *PI* parameter consistently exceeding 99.8%.

$$PI = \left(1 - \frac{t_{cs}}{t_{ps}}\right) \tag{19}$$

The computational time was significantly decreased from approximately 2 s to around 2e−3 s by implementing a non-optimized code in Matlab®. With further optimization through the use of lower level programming languages, additional reductions in computational time are likely to be achieved. This significant increment in computation efficiency suggests the possibility of using the CP method also for complex geometries, when the critical locations are not known in advance.

It is worth noting that if any of the assumptions given in Section 4 is not holding (e.g., in presence of residual stresses, non proportional loading, plasticity), a correct closed-form solution cannot be obtained. Figure 7 provides a practical example in which non-proportional loading conditions were applied to the hourglass specimen, notched specimen and the welded joint. The non proportional loading conditions are reported in Table 6 and are identified as *Case 3*. Under these conditions a significant difference can be found both in terms of *FS* parameter and critical plane orientations, as shown in Table 7. As it can be observed, the obtained parameter

TABLE 5 Comparison of computational cost between the closed-form solution and the standard plane scanning method.

Computational time comparison									
	Hourglass specimen			Notched specimen			Welded joint		
Load type	t_{cs}	t_{ps}	*PI*	t_{cs}	t_{ps}	*PI*	t_{cs}	t_{ps}	*PI*
Case 1	2.15e−3 s	2.21 s	99.9%	2.84e−3 s	2.006 s	99.8%	2.47e−3 s	1.849 s	99.8%
Case 2	1.822e−3 s	2.27 s	99.9%	1.985e−3 s	2.282 s	99.9%	2.04e−3 s	2.164 s	99.9%

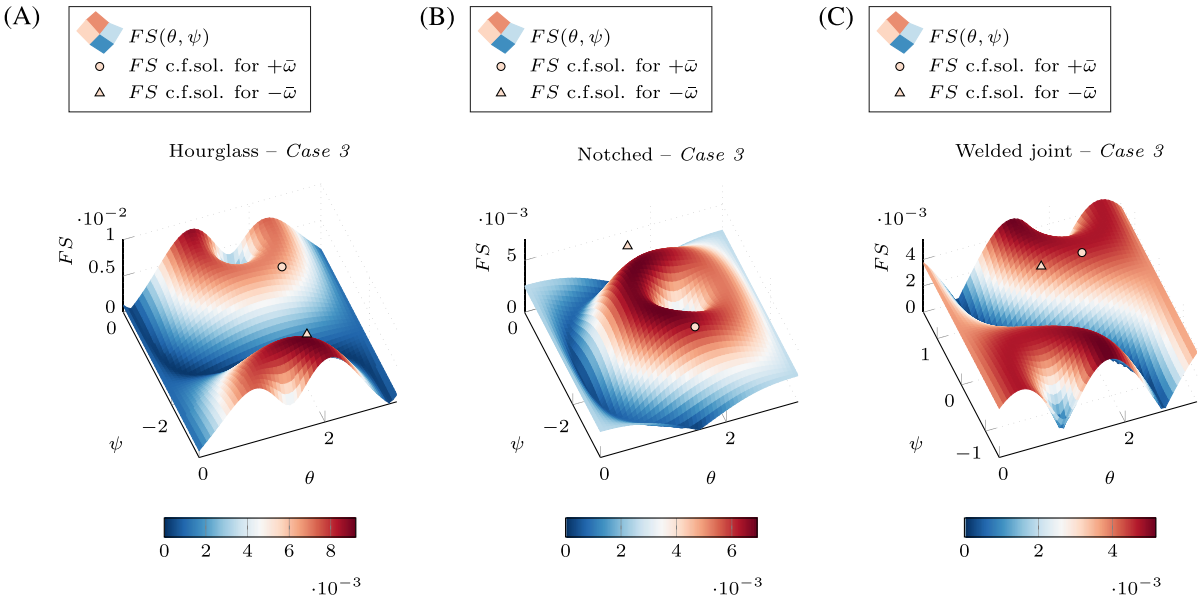

FIGURE 7 Comparison of *FS* solutions between the standard plane scanning method $FS(\theta,\psi)$ and that derived from the closed-form solution (i.e., c.f.sol.) *FS* for (A) the hourglass specimen subjected to non proportional tensile-torsion loading, (B) the notched specimen subjected to non proportional tensile-torsion loading, and the welded joint subjected to non proportional bending-torsion loading. [Colour figure can be viewed at wileyonlinelibrary.com]

TABLE 6 Load steps combination used during simulations to apply non-proportional loading conditions, with F, F_1 and F_2 referring to the applied forces and M_t referring to the torque shown in Figure 5.

	Hourglass specimen		Notched specimen		Welded joint	
Load type	Load step n.1	Load step n.2	Load step n.1	Load step n.2	Load step n.1	Load step n.2
Case 3	$F = 140$ kN	$F = 0$ kN	$F = 53$ kN	$F = 0$ kN	$F_1 = 3.4$ kN	$F_1 = -11$ kN
	$M_t = 0$ N m	$M_t = 100$ N m	$M_t = 0$ N m	$M_t = 80$ N m	$F_2 = 3.4$ kN	$F_2 = 11$ kN

TABLE 7 Comparison of *FS* values and critical plane orientations between the closed-form solution and the standard plane scanning method for non-proportional loading conditions.

FS comparison ($\pm\bar{\omega}$)						
	Hourglass specimen		Notched specimen		Welded joint	
Load type	Closed-form	Standard	Closed-form	Standard	Closed-form	Standard
Case 3	8.12e−3	9.23e−3	6.81e−3	6.91e−3	4.82e−3	5.17e−3

(Continues)

TABLE 7 (Continued)

θ and ψ comparison ($+\overline{\omega}$)												
	Hourglass specimen				**Notched specimen**				**Welded joint**			
	Closed-form		**Standard**		**Closed-form**		**Standard**		**Closed-form**		**Standard**	
Load type	θ	ψ	θ	ψ	θ	ψ	θ	ψ	θ	ψ	θ	ψ
Case 3	2.10	−1.096	1.822	−2.76	1.745	−2.51	1.382	−2.07	2.17	0.657	1.759	−1.382
θ and ψ comparison ($-\overline{\omega}$)												
	Hourglass specimen				**Notched specimen**				**Welded joint**			
	Closed-form		**Standard**		**Closed-form**		**Standard**		**Closed-form**		**Standard**	
Load type	θ	ψ	θ	ψ	θ	ψ	θ	ψ	θ	ψ	θ	ψ
Case 3	2.16	−0.304	1.822	−2.76	1.395	−0.631	1.382	−2.07	1.506	0.615	1.759	−1.382

FS is always smaller than the one obtained by means of the plane scanning method.

7 | CONCLUSIONS

Following a previous work by the authors, the purpose of the present study was to develop a closed-form solution for the *Fatemi-Socie* CP factor in its extended formulation, that is, including the shear strain range and the maximum normal stress acting on the plane during the loading cycle. The method utilizes stress and strain tensor invariants and coordinates transformation law and was implemented in a readily available Matlab® script. The closed-form solution was discussed with reference to its graphical representation for a structural steel, and similar solutions can be easily obtained for different metallic materials. Various case studies were analyzed and discussed in comparison to the standard plane scanning method, to provide a wide range of component geometries and loading conditions. From the performed analyses and results obtained, the following conclusions can be drawn:

- the method can be used for uniaxial and multiaxial proportional loading conditions, under linear-elastic material behavior;
- the method offers a significant speed up in solution time, with respect to the standard plane scanning method, with a reduction of computation time greater than 99.8% on a single node, for the examined test cases, where a 1° resolution in plane orientation was selected; this reduction in computation time could potentially make CP methods easier and more attractive to be used, even in an industrial context;
- the proposed method provides a closed-form solution for the critical plane and, consequently, for the damage parameter, compared to the standard plane scanning method;
- the developed analytical formulation provides an more in depth understanding of critical plane orientation; in particular, it was discussed that in general, for a three-dimensional state of stress, there are at least two critical plane orientations, while infinite orientations can be obtained in case of two identical eigenvalues of the strain range tensor, and four critical planes exist in case of equal and opposite eigenvalues of the stress tensor;
- the method is easy to use and can be implemented in a variety of codes since it utilizes basic tensor math; the extension to other CP factors likely appears to be straightforward.

Reducing computation time during the post-processing phase is crucial for evaluating damage factors, as it enables a more detailed and complete evaluation of the studied model, even in case of complex geometries with FE models made with large number of nodes.

NOMENCLATURE

$\alpha_1, \alpha_2, \alpha_3$	eigenvalues
$\overline{\omega}$	angle by which the principal reference frame is to be rotated
$\Delta\varepsilon^{(i,i+1)}$	strain range tensor between the i-th and $i+1$-th load steps
$\boldsymbol{\sigma}'$	rotated stress tensor
$\boldsymbol{\sigma}$	stress tensor
$\boldsymbol{\sigma}^{(i)}$	stress tensor at the i-th load step
$\boldsymbol{\varepsilon}'$	rotated strain tensor
$\boldsymbol{\varepsilon}$	strain tensor
$\boldsymbol{\varepsilon}^{(i)}$	strain tensor at the i-th load step
$\boldsymbol{n_j}^{(i),(i+1)}$	j-th principal direction of the strain range tensor

$\Delta\gamma$	range of shear strain
$\Delta\theta$, $\Delta\psi$	fixed angular increment
γ_{ij}	shear strain
ν	Poisson's ratio
ω	angle of the principal reference frame rotation
σ_{ii}	normal stress
$\sigma_{n,max}$	maximum normal stress
τ_{ij}	shear stress
θ, ψ	standard scanning plane angles
ε_{ii}	normal strain
$abcd$	closed-form solution parameters
E	Young's modulus
F	force
FS	*Fatemi-Socie* critical plane parameter
k	*Fatemi-Socie* material constant
M_t	torque
$Oxyz$	reference coordinate system
R	rotation matrix
R_i	rotation matrix about i-axis
S_y	yield strength
t_{cs}	computation time for the closed-form solution
t_{ps}	computation time for the plane scanning procedure
PI	performance index
CP	critical plane
FEA	finite element analysis
FEM	finite element model

ACKNOWLEDGMENTS

This study was financed by the European Union – NextGenerationEU (National Sustainable Mobility Center CN00000023, Italian Ministry of University and Research Decree n. 1033 – 17/06/2022, Spoke 11 – Innovative Materials & Lightweighting). The opinions expressed are those of the authors only and should not be considered as representative of the European Union or the European Commission's official position. Neither the European Union nor the European Commission can be held responsible for them.

DATA AVAILABILITY STATEMENT

A Matlab® script that implements the closed-form algorithm reported in the article has been uploaded to a GitHub repository: https://github.com/achiocca1/FS-Sol. For ease of use, the folder includes the nodal results of the tensile loaded notched specimen.

ORCID

Andrea Chiocca https://orcid.org/0000-0002-1472-4398
Michele Sgamma https://orcid.org/0009-0003-8637-9946
Francesco Frendo https://orcid.org/0000-0002-7472-4664

REFERENCES

1. Bhaumik SK, Sujata M, Venkataswamy MA. Fatigue failure of aircraft components. *Eng Fail Anal*. 2008;15(6):675-694.
2. Kuncham E, Sen S, Kumar P, Pathak H. An online model-based fatigue life prediction approach using extended Kalman filter. *Theor Appl Fract Mech*. 2022;117:103143.
3. Chen F, Shang D-G, Li D-H, Wang L-W. Multiaxial thermo-mechanical fatigue life prediction based on notch local stress-strain estimation considering temperature change. *Eng Fract Mech*. 2022;265:108384.
4. Chiocca A, Frendo F, Bertini L. Evaluation of residual stresses in a tube-to-plate welded joint. *MATEC Web of Conf*. 2019;300:19005.
5. Chiocca A, Frendo F, Bertini L. Evaluation of residual stresses in a pipe-to-plate welded joint by means of uncoupled thermal-structural simulation and experimental tests. *Int J Mech Sci*. 2021;199:106401.
6. Frendo F, Marulo G, Chiocca A, Bertini L. Fatigue life assessment of welded joints under sequences of bending and torsion loading blocks of different lengths. *Fract Eng Mater Struct*. 2020;43(6):1290-1304.
7. Meneghetti G, Campagnolo A, Visentin A, et al. Rapid evaluation of notch stress intensity factors using the peak stress method with 3D tetrahedral finite element models: comparison of commercial codes. *Fract Eng Mater Struct*. 2022;45(4):1005-1034.
8. Palmieri M, Zucca G, Morettini G, Landi L, Cianetti F. Vibration fatigue of FDM 3D printed structures: the use of frequency domain approach. *Materials*. 2022;15(3):854.
9. Berto F, Lazzarin P. The volume-based strain energy density approach applied to static and fatigue strength assessments of notched and welded structures. *Procedia engineering*, Vol. 1: No longer published by Elsevier; 2009:155-158.
10. Lazzarin P, Berto F. Some expressions for the strain energy in a finite volume surrounding the root of blunt V-notches. *Int J Fract*. 2005;135(1-4):161-185.
11. Mroziński S. Energy-based method of fatigue damage cumulation. *Int J Fatigue*. 2019;121:73-83.
12. Varvani-Farahani A, Haftchenari H, Panbechi M. An energy-based fatigue damage parameter for off-axis unidirectional FRP composites. *Compos Struct*. 2007;79(3):381-389.
13. European Committee for Standardization. Eurocode 3: Design of steel structures – Part 1-9: Fatigue. *(CEN)*. 2005;50:77.
14. Findley WN. A theory for the effect of mean stress on fatigue of metals under combined torsion and axial load or bending. *J Eng Ind*. 1959;81(4):301-305.
15. Hobbacher AF. The new IIW recommendations for fatigue assessment of welded joints and components—a comprehensive code recently updated. *Int J Fatigue*. 2009;31(1):50-58.
16. Kandil FA, Brown MW, Miller KJ. *Biaxial low-cycle fatigue failure of 316 stainless steel at elevated temperatures*. Metals Society; 1982.
17. Karakaş, Zhang G, Sonsino CM. Critical distance approach for the fatigue strength assessment of magnesium welded joints in contrast to Neuber's effective stress method. *Int J Fatigue*. 2018;112:21-35.
18. Radaj D, Sonsino CM, Fricke W. *Fatigue Assessment of Welded Joints by Local Approaches*. 2nd ed.: Woodhead Publishing; 2006.

19. Socie D. Multiaxial fatigue damage models. *J Eng Mater Technol*. 1987;109(4):293-298.
20. Taylor D, Barrett N, Lucano G. Some new methods for predicting fatigue in welded joints. *Int J Fatigue*. 2002;24(5):509-518.
21. Cruces AS, Garcia-Gonzalez A, Moreno B, Itoh T, Lopez-Crespo P. Critical plane based method for multiaxial fatigue analysis of 316 stainless steel. *Theor Appl Fract Mech*. 2022;118:103273.
22. Cruces AS, Lopez-Crespo P, Moreno B, Antunes FV. Multiaxial fatigue life prediction on S355 structural and offshore steel using the SKS critical plane model. *Metals*. 2018;8(12):1060.
23. El-sayed HM, Lotfy M, El-din Zohny HN, Riad HS. Prediction of fatigue crack initiation life in railheads using finite element analysis. *Ain Shams Eng J*. 2018;9(4):2329-2342.
24. Huang J, Yang X, Shi D, Yu H, Dong C, Hu X. Systematic methodology for high temperature LCF life prediction of smooth and notched Ni-based superalloy with and without dwells. *Comput Mater Sci*. 2014;89:65-74.
25. Reis L, Li B, De Freitas M. A multiaxial fatigue approach to rolling contact fatigue in railways. *Int J Fatigue*. 2014;67:191-202.
26. Marques JME, Benasciutti D, Carpinteri A, Spagnoli A. An algorithm for fast critical plane search in computer-aided engineering durability analysis under multiaxial random loadings: application to the Carpinteri–Spagnoli–Vantadori spectral method. *Fract Eng Mater Struct*. 2020;43(9):1978-1993.
27. Wentingmann M, Noever-Castelos P, Balzani C. An adaptive algorithm to accelerate the critical plane identification for multiaxial fatigue criteria. In: Proceedings of the 6th European Conference on Computational Mechanics: Solids, Structures and Coupled Problems, ECCM 2018 and 7th European Conference on Computational Fluid Dynamics, ECFD 2018; 2020:3745-3754.
28. Sunde SL, Berto F, Haugen B. Efficient implementation of critical plane for 3D stress histories using triangular elements. *Int J Fatigue*. 2020;134:105448.
29. Albinmousa J, Al Hussain M. Polar damage sum concept for constant amplitude proportional and nonproportional multiaxial fatigue analysis. *Forces Mech*. 2021;4:100025.
30. Liu J, Ran Y, Wei Y, Zhang Z. A critical plane-based multiaxial fatigue life prediction method considering the material sensitivity and the shear stress. *Int J Press Vessels Pip*. 2021;194:104532.
31. Ma T-H, Zhou C-Y, Gao N, Chang L, He X-H. Low cycle fatigue behavior of CP-Ti under multiaxial load-controlled mode at different multiaxial stress ratios. *Int J Fatigue*. 2022;160:106868.
32. Chiocca A, Frendo F, Marulo G. An efficient algorithm for critical plane factors evaluation. *Int J Mech Sci*. 2023;242:107974.
33. Jiang Y, Hertel O, Vormwald M. An experimental evaluation of three critical plane multiaxial fatigue criteria. *Int J Fatigue*. 2007;29(8):1490-1502.
34. Fatemi A, Socie DF. A critical plane approach to multiaxial fatigue damage including out-of-phase loading. *Fract Eng Mater Struct*. 1988;11(3):149-165.
35. Fatemi A, Kurath P. Multiaxial fatigue life predictions under the influence of mean-stresses. *J Eng Materials Technol Trans ASME*. 1988;110(4):380-388.
36. Olausson K. Material data derivation for the Fatemi And Socie critical plane method. *Ph.D. Thesis*, Luleå University of Technology; 2007.
37. Lopez-Crespo P, Moreno B, Lopez-Moreno A, Zapatero J. Study of crack orientation and fatigue life prediction in biaxial fatigue with critical plane models. *Eng Fract Mech*. 2015;136:115-130.
38. Yang S, Sun J. Multiaxial fatigue life assessment of 304 austenitic stainless steel with a novel energy-based criterion. *Int J Fatigue*. 2022;159:106728.
39. Yu ZY, Zhu SP, Liu Q, Liu Y. Multiaxial fatigue damage parameter and life prediction without any additional material constants. *Materials*. 2017;10(8):923.
40. Zhu SP, Yu ZY, Correia J, De Jesus A, Berto F. Evaluation and comparison of critical plane criteria for multiaxial fatigue analysis of ductile and brittle materials. *Int J Fatigue*. 2018;112:279-288.
41. Chiocca A, Sgamma M, Frendo F, Bucchi F. Rapid and accurate fatigue assessment by an efficient critical plane algorithm: application to a FSAE car rear upright. *Proc Structu Integr*. 2023;47:749-756.
42. Chiocca A, Frendo F, Bertini L. Experimental evaluation of relaxed strains in a pipe-to-plate welded joint by means of incremental cutting process. *Procedia Struct*. 2020;28:2157-2167.
43. Chiocca A. Influence of residual stresses on the fatigue life of welded joints. *Ph.D. Thesis*, University of Pisa; 2021.
44. Chiocca A, Frendo F, Aiello F, Bertini L. Influence of residual stresses on the fatigue life of welded joints. Numerical simulation and experimental tests. *Int J Fatigue*. 2022;162:106901.
45. Chiocca A, Frendo F, Bertini L. Evaluation of heat sources for the simulation of the temperature distribution in gas metal arc welded joints. *Metals*. 2019;9(11):1142.

How to cite this article: Chiocca A, Sgamma M, Frendo F. Closed-form solution for the *Fatemi-Socie* extended critical plane parameter in case of linear elasticity and proportional loading. *Fatigue Fract Eng Mater Struct*. 2024;47(1):72-87. doi:10.1111/ffe.14153